ResearchGate

See discussions, stats, and author profiles for this publication at: https://www.researchgate.net/publication/272192224

Mechanism and Dynamics of Electron Injection and Charge Recombination in DNA. Dependence on Neighboring Pyrimidines

ARTICLE *in* THE JOURNAL OF PHYSICAL CHEMISTRY B · FEBRUARY 2015

Impact Factor: 3.3 · DOI: 10.1021/jp512113w · Source: PubMed

CITATIONS
2

READS
34

6 AUTHORS, INCLUDING:

Arjan J Houtepen
Delft University of Technology
68 PUBLICATIONS **1,472** CITATIONS
SEE PROFILE

F.C. Grozema
Delft University of Technology
129 PUBLICATIONS **3,719** CITATIONS
SEE PROFILE

Frederick D Lewis
Northwestern University
319 PUBLICATIONS **9,207** CITATIONS
SEE PROFILE

Available from: F.C. Grozema
Retrieved on: 25 January 2016

THE JOURNAL OF PHYSICAL CHEMISTRY B

Article

pubs.acs.org/JPCB

Mechanism and Dynamics of Electron Injection and Charge Recombination in DNA. Dependence on Neighboring Pyrimidines

Natalie Gorczak,[§,∥] Taiga Fujii,[†,∥] Ashutosh Kumar Mishra,[†] Arjan J. Houtepen,[§] Ferdinand C. Grozema,*[,§] and Frederick D. Lewis*[,†]

[§]Department of Chemical Engineering, Delft University of Technology, 2628 BL Delft, The Netherlands

[†]Department of Chemistry, Northwestern University, Evanston, Illinois 60208-3113, United States

Supporting Information

ABSTRACT: The mechanism and dynamics of photoinduced electron injection and charge recombination have been investigated for several series of DNA hairpins. The hairpins possess a stilbenediether linker, which serves as an electron donor and base pair stems that possess different pyrimidine bases adjacent to the linker. Hairpins with adjacent thymine-adenine (T-A) base pairs undergo fast electron injection and relatively slow charge recombination with rate constants that are not strongly dependent upon the following base pair. Hairpins with adjacent cytosine-guanine (C-G) base pairs undergo reversible electron injection and much faster charge recombination than those with adjacent T-A base pairs. Hairpins with 5-fluorouracil or other halogenated pyrimidines in their first and second base pair undergo fast electron injection and multiexponential charge recombination. The difference in kinetic behavior for the different series of hairpins and its implications for the formation of long-lived charge-separated states are discussed and compared to results reported previously for other electron-donor chromophores.

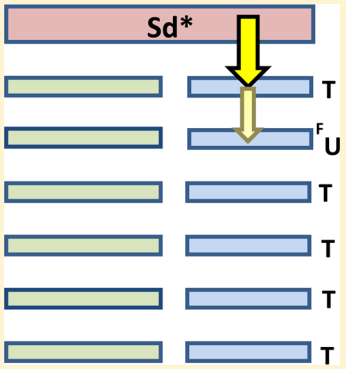

INTRODUCTION

The mechanism and dynamics of charge transport over long distances in organic molecules including DNA continues to attract the interest of both experimental and theoretical scientists.[1−4] Recent reviews provide extensive information about the base sequence dependence of the dynamics of the transport of positive charge (holes) in DNA but make scant mention of excess electron-transport dynamics.[5,6] There is ample evidence for the occurrence of electron transport over multiple base pairs in low or undetermined quantum yield using methods based on chemical detection, including loss of bromide ion from bromouracil and reductive splitting of thymine dimer.[7−12] However, a recent claim of faster electron versus hole transport in DNA[13] is not consistent with earlier reports and with the failure to observe arrival of an electron at a trap site when the electron donor and acceptor are separated by more than a few intervening adenine-thymine (A-T) base pairs.[13−17]

Our studies of photoinduced charge separation in DNA have led to the conclusion that the initial steps in many hole-transport processes are the formation of a radical ion pair or exciplex between a covalently attached electron acceptor and an adjacent purine base followed by the transport of the hole to the closest hole trap, which can either be a base of low oxidation potential such as guanine or deazaguanine or a second chromophore that serves as a hole trap.[6,18] Several mechanisms have been proposed for the hole-transport process, including the more traditional tunneling and incoherent hopping and the recently proposed quantum filling and flickering resonance.[19−23]

One of us has been involved in several attempts to study the analogous initial steps in the electron-transport process. Studies of photoinduced charge transfer in a DNA hairpin possessing a stilbenediether **Sd** linker and a poly(T-A) stem (**T6**, Chart 1a,c) have shown that it undergoes rapid electron injection followed by fast charge recombination (∼1 and 30 ps, respectively), with no evidence for a slow component of charge recombination.[24,25] Similar results were obtained for **Sd**-linked hairpins with neighboring cytosine-guanine (C-G) or ^{Br}U-A base pair (Chart 1b). We subsequently investigated the dynamics of electron injection in hairpins having an aminopyrene **APy** capping group (Chart 1a) and a poly(T-A) stem containing a single ^{Br}U-A base pair at variable locations with respect to **APy**.[9] Fujisuka and Majima have investigated the dynamics of electron injection and charge recombination in hairpins having a dithiophene linker (**TT**, Chart 1a) and either poly(A-T) or poly(G-C) stems.[26,27]

Recently, Ito and co-workers have reported that the chemical yields for photoinduced loss of bromide ion from ^{Br}U is enhanced when a charge gradient consisting of T, U, ^{F}U, and ^{Br}U is employed for electron transport from singlet phenothiazine.[28] Purine oxidation potential gradients have previously been used to enhance the quantum yields and dynamics of hole transport in DNA;[29,30] however, pyrimidine reduction potential gradients have not been used to systematically investigate the dynamics of photoinduced electron transport in DNA. We report here the results of an investigation of the dynamics of electron

Special Issue: John R. Miller and Marshall D. Newton Festschrift

Received: December 4, 2014
Revised: February 4, 2015
Published: February 10, 2015

ACS Publications © 2015 American Chemical Society

DOI: 10.1021/jp512113w
J. Phys. Chem. B 2015, 119, 7673−7680

Chart 1. (a) Structures, Excitation Energies, and Ground- and Excited-State Oxidation Potentials of the Electron Donors Sd,[24] APy,[9] and TT;[27] (b) Structures and Reduction Potentials[a] of Natural and Halogenated Pyrimidine Bases and Structures of Sd-linked Hairpins Possessing (c) (T-A) Neighboring Base Pairs, (d) (C-G) Neighboring Base Pairs, or (e) Halogenated Uracils

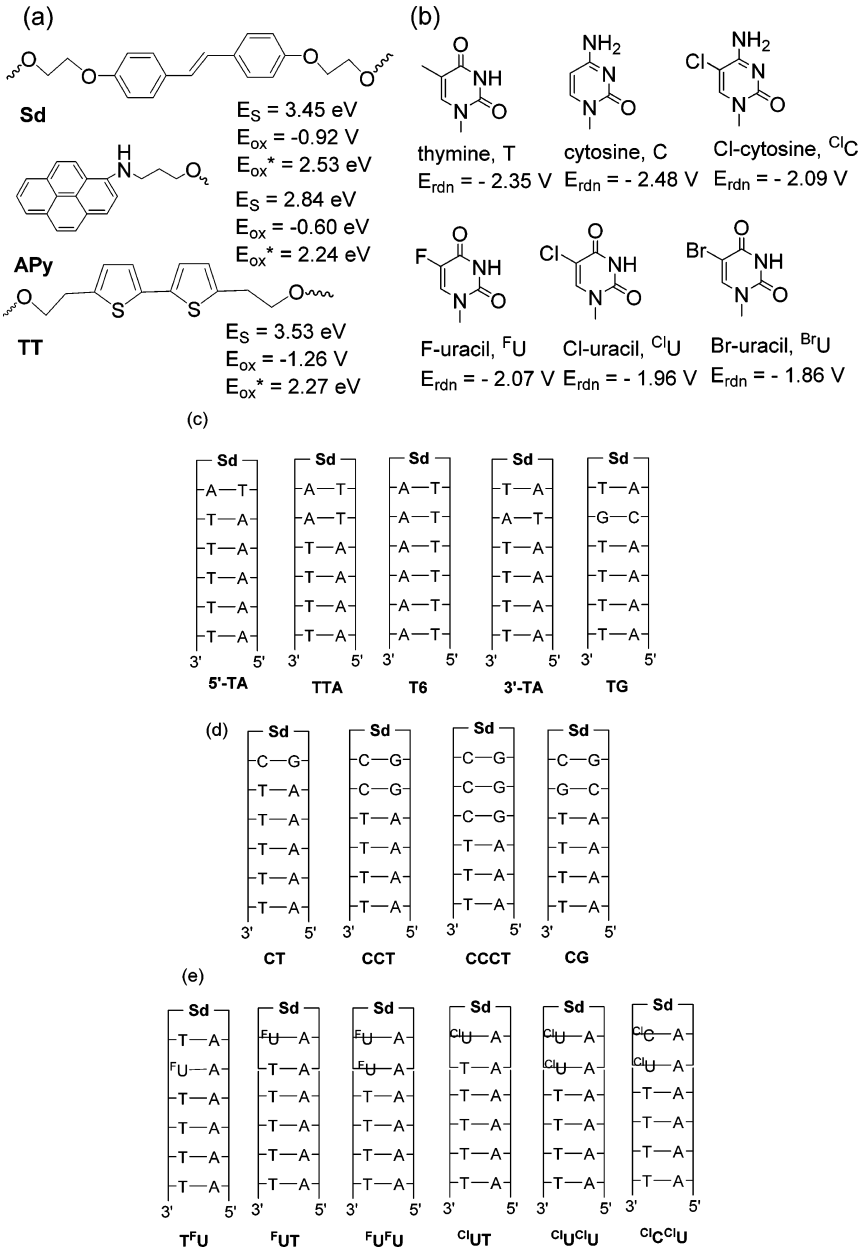

[a]See the Experimental Section.

injection and charge recombination in three series of **Sd**-linked hairpins (Chart 1). The first two series possess only T-A and C-G base pairs arranged in different orders with the T-A base pair adjacent to the **Sd** linker in series T-A (Chart 1c) and the C-G base pair in series C-G (Chart 1d). The third series possesses either one or two ^{F}U-A or ^{Cl}U-A base pairs (Chart 1e). We observe distinctive differences in the kinetic behavior of the three series.

EXPERIMENTAL SECTION

Materials. The stilbenediether diol (**Sd**) was prepared by the method of Sieber[31] and converted to its mono-(dimethoxytrityl) derivative and hence to its cyanoethyl-*N*,*N*-diisopropylphosphoramidite derivative by the method of Letsinger and Wu.[32] 5-Chloro-2′-deoxycytosine (^{Cl}C) and 5-chloro-2′-deoxyuridine (^{Cl}U) phosphoramidite monomers were synthesized following published procedures.[33,34] The hairpins shown in Chart 1 were prepared by means of standard solid-supported phosporamidite chemistry following the procedure of Letsinger and Wu,[32] purified to a single peak by reverse phase HPLC (Figure S1, Supporting Information), and characterized by their UV and circular dichroism (CD) spectra (Figures S2 and S3, Supporting Information) and mass spectrometry (Table S1, Supporting Information). Representative thermal dissociation profiles are shown in Figure S4 (Supporting Information).

Methods. *Transient Absorption Spectroscopy.* Pump−probe transient absorption measurements were performed using a

DOI: 10.1021/jp512113w
J. Phys. Chem. B 2015, 119, 7673−7680

Scheme 1. Kinetic Schemes for (a) T-A Hairpin Series, (b) C-G Hairpin Series, and (c) Halouracil Series Hairpin T^{F}U

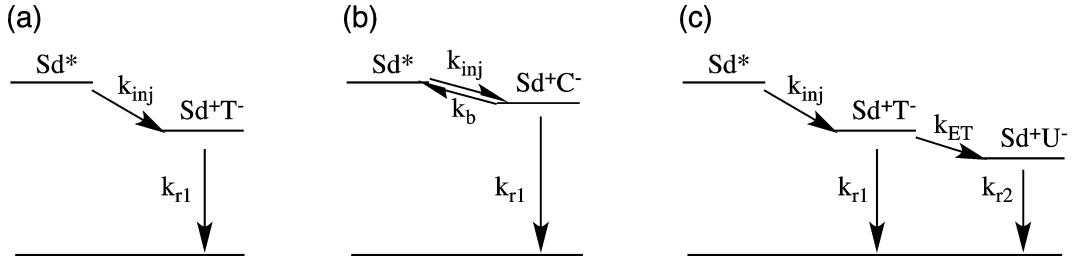

tunable laser system comprising a Yb:KGW laser (1028 nm) operating at 5 kHz with a pulse duration of 180 fs (PHAROS-SP-06-200, Light Conversion) and an optical parametric amplifier (ORPHEUS-PO15F5HNP1, Light Conversion). White light continuum probe pulses were generated by focusing the fundamental on a sapphire crystal. Data were acquired using a transient absorption spectrometer (HELIOS, Ultrafast Systems). Samples were placed in quartz cuvettes with a 2 mm path length and stirred with a magnetic stirrer throughout the experiments. The samples were excited at 330 nm with pulses of 80 nJ and a 200 μm spot size in quasi-parallel pump−probe geometry. The two-dimensional data were analyzed with global and target analysis utilizing the open-source software Glotaran,[35] a graphical user interface for the R package TIMP.[36] TIMP is based on spectrotemporal parametrization assuming that the time-dependent spectra are linear combinations of transient absorption spectra of the various species with their respective population profiles.[37] To model the photophysical processes after excitation, target analysis was applied with the respective compartmental kinetic schemes depicted in Scheme 1. Dispersion in the data was modeled with a parametrized Gaussian instrument response function. Applying a correct scheme yields transient absorption spectra of the excited or radical ion states involved in the photophysical processes (referred to as species-associated spectra) together with their population profiles. The quality of the fits was therefore not only examined on the basis of the residuals but also on the meaningfulness of the species-associated spectra. In particular, analysis of each data set should result in comparable species-associated spectra of the excited Sd state (Sd*) and the radical cation state (Sd$^{+\bullet}$). Small deviations are possible due to different chemical surrounding that can induce slight shifts of transition energies or change in the oscillator strength.

Electrochemical Reduction Potentials. The reduction potentials for the deoxynucleosides ^{F}U, ^{Cl}U, and ^{Cl}C were measured in dimethylformamide solution containing 0.1 M tetra-*n*-butylammonium hexafluorophosphate versus Ag/AgCl by means of cyclic voltammetry using ferrocene/ferrocinium as the internal standard. Values reported in Chart 1b versus SCE along with previously reported values for T and C are peak potentials for irreversible reduction.[9]

RESULTS

Synthesis, Absorption, and Fluorescence Spectra. The hairpins in Chart 1c−e were synthesized, purified, and characterized using the methods described in the Experimental Section. The hairpins are named so as to identify the first two or three bases in the same hairpin arm as the pyrimidine base adjacent to the linker. Only in the cases of hairpins containing six consecutive T's or three consecutive C's are more than three bases specified in the name. The first pyrimidine is located in the 3′-arm of the hairpin, except as noted in Chart 1c−e and, when relevant, in the text.

As previously reported, the **Sd** has absorption and fluorescence maxima at 326 and 374 nm, respectively, in methanol, with a fluorescence quantum yield of 0.32 and a decay time of 350 ps.[38] The UV spectra of all of the hairpins in aqueous buffer consist of a long-wavelength band near 327 nm assigned to the stilbene chromophore and a stronger band near 260 nm assigned to the overlapping absorption of the nucleobases and the stilbene (Figure S2, Supporting Information). All of the **Sd** hairpins are very weakly fluorescent ($\Phi_f < 10^{-3}$). DNA duplexes containing 5-fluorouracil (^{F}U-A),[39,40] 5-chlorouracil (^{Cl}U-A),[41] and 5-chlorocytosine (^{Cl}C-G)[42] base pairs are reported to adopt normal B-DNA structures and have thermodynamics stabilities similar to or greater than those of duplexes having nonhalogenated base pairs. The melting temperatures of hairpins **T^{F}U** and **^{Cl}UT** (~70 °C, Figure S4 (Supporting Information)) are somewhat higher than that of hairpin **T6** (64 °C).[38]

Transient Absorption Spectra. Time-resolved transient absorption spectra for the **Sd** hairpins were obtained using a Yb:KGW-based laser system with a time resolution of ~200 fs in the spectral window of 500−900 nm. The time-resolved spectra obtained from such measurements for hairpin **T6** upon excitation at 330 nm are shown in Figure 1a. The band at around 575 nm (previously assigned to Sd*)[24] decays rapidly, accompanied by the rise and subsequent decay of bands at around 535 and 860 nm. The band at 535 nm was previously assigned to Sd$^{+\bullet}$, whereas the one at 860 nm was not previously observed because of limited long-wavelength detection in transient absorption measurements.[24,43] The observed behavior is consistent with simple sequential kinetics, as shown in Scheme 1a. The species-associated spectra for Sd* and Sd$^{+\bullet}$ obtained from target analysis of the two-dimensional data are shown in Figure 1b. The spectrum for Sd$^{+\bullet}$ is similar to those previously obtained for *trans*-stilbene derivatives by spectroelectrochemistry[44] or pulse radiolysis.[45,46]

Single-wavelength kinetic traces and population profiles obtained from target analysis are shown in Figure S5a (see the Supporting Information). This figure shows that the band at 860 nm directly represents the kinetics of formation and decay of Sd^{+} because there is no overlap with other species in this spectral range. The population profiles provide values of k_{inj} and k_{r1} for formation and decay of the Sd$^{+\bullet}$/T$^{-\bullet}$ radical ion pair reported in Table 1. Similar time-resolved spectra (Figure S6a−d, Supporting Information) and kinetic behavior were observed for hairpins 5′-**TA**, 3′-**TA**, **TTA**, and **TG**, all of which possess a T-A base pair adjacent to the Sd linker (Chart 1c). The rise and decay of Sd$^{+\bullet}$ monitored at 860 nm are shown in Figure 2, and rate constants for charge injection and charge recombination obtained from target analysis for the T-A series hairpins are

DOI: 10.1021/jp512113w
J. Phys. Chem. B 2015, 119, 7673−7680

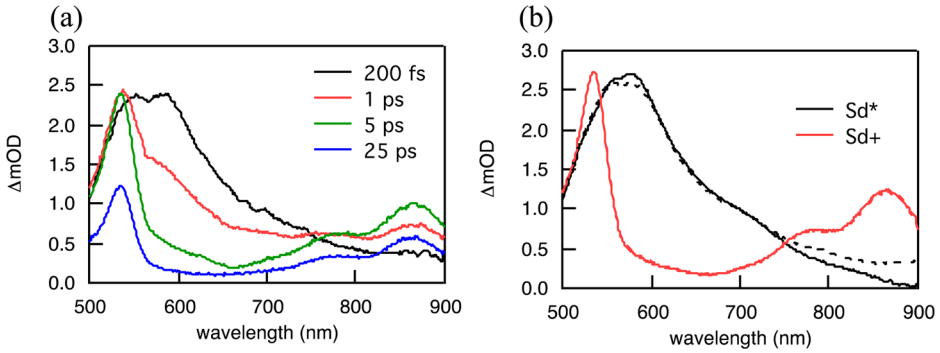

Figure 1. (a) Time-resolved spectra for hairpin **T6** and (b) species-associated spectra obtained from target analysis for hairpin **T6**. The dashed lines are the species-associated spectra resulting from the simultaneous target analysis for hairpins **T6** and **CT**.

Table 1. Rate Constants for the Photophysical Processes Occurring upon Excitation of the Sd-Linked Hairpins[a,b] along with the Quantum Yield of Electron Transfer Subsequent to Electron Injection, $\Phi_{ET} = k_{ET}/(k_{ET} + k_{r1})$, for the Halo-U Series

hairpin	k_{inj}, ps^{-1}	k_b, ps^{-1}	k_{r1}, ps^{-1}	k_{ET}, ps^{-1}	k_{r2}, ps^{-1}	Φ_{ET}
5′-**TA**	0.59		0.038			
TTA	0.71		0.034			
T6	0.64		0.034			
3′-**TA**	0.54		0.054			
TG	0.41		0.041			
CT	0.46	0.31	0.37			
CCT	0.43	0.54	0.36			
CCCT	0.43	0.57	0.35			
CG	0.45	0.42	0.22			
$\mathbf{T^FU}$	0.87		0.069	0.024	0.012	0.26
$\mathbf{^FUT}$	1.9		0.17	0.057	0.034	0.25
$\mathbf{^FU^FU}$	2.5		0.15	0.011	0.033	0.07
$\mathbf{^{Cl}UT}$	1.2	0.22	0.12	0.13	0.032	0.28
$\mathbf{^{Cl}U^{Cl}U}$	2.9		0.12	0.012	0.028	0.09
$\mathbf{^{Cl}C^{Cl}U}$	2.4		0.40	0.018	0.011	0.04

[a]Rate constants were obtained by applying target analysis to the two-dimensional transient absorption data using Scheme 1a for the T-A series, Scheme 1b for the C-G series, and Scheme 1c for the halo-U series. The uncertainty for the fastest rates (2−3 ps^{-1}) is estimated to be no worse than 0.4 ps^{-1} (20%) and substantially less than this for the slower rates. [b]See Chart 1c−e for hairpin structures.

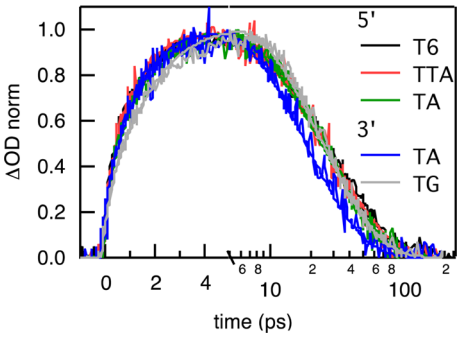

Figure 2. $Sd^{+\bullet}$ formation and decay for hairpins in the T-A series monitored at 860 nm. See Chart 1c for hairpin structures.

reported in Table 1. There are only minor differences in the values of k_{inj} and k_{r1} for these hairpins.

Time-resolved spectra for hairpin **CT** are shown in Figure 3a. The rise of the 525 and 860 nm bands is similar to that for **T6** (Figure 1a); however, the decay of the band at 575 nm is much slower than that for **T6**. All three absorption bands decay in parallel rather than sequentially. This behavior, which is observed for all of the hairpins in Chart 1d (Figure S6e−g, Supporting Information), is indicative of reversible electron injection with a rate constant k_b, as shown in Scheme 1b. The simultaneous fit of the data sets for **CT** to Scheme 1b and for **T6** to Scheme 1a provides species-associated spectra for Sd* and $Sd^{+\bullet}$ (dashed lines, Figure 1b) nearly identical to those for **T6** alone. Kinetic traces and population profiles are provided in Figure S5b (Supporting Information). The rise and decay of $Sd^{+\bullet}$ monitored at 860 nm for the hairpins having a C-G base pair adjacent to **Sd** are shown in Figure 4a, and rate constants for electron injection, back transfer, and recombination obtained from target analysis are reported in Table 1. Values of k_{inj}, k_b, and k_{r1} are independent of the number of sequential C-G base pairs. When the second base pair is inverted in the case of hairpin **CG**, the rate constant for charge recombination (k_{r1}) is somewhat slower; however, the rate constants for electron injection and back transfer are similar to those for **CT**.

The time-resolved spectra for $\mathbf{^FUT}$ are shown in Figure 3b and for the other halo-pyrimidine-containing hairpins in Figure S6h−l (Supporting Information). Kinetic traces for $\mathbf{^FUT}$ and $\mathbf{^FU^FU}$ at several wavelengths are provided in Figure S5b (Supporting Information). The rise and decay of the 860 nm bands for $\mathbf{^FUT}$, $\mathbf{^FU^FU}$, and $\mathbf{T^FU}$ and the $\mathbf{^{Cl}U}$- and $\mathbf{^{Cl}C}$-containing hairpins are shown in Figure 4b. Disappearance of the 575 nm Sd* band is much faster for the halo-U series than that for any of the T-A series hairpins (cf. Figure 1a). This is also the case for $\mathbf{T^FU}$, which has a T-A base pair adjacent to **Sd**. The decay of the 860 nm bands for the halo-U series does not display monoexponential behavior. Therefore, Scheme 1c is applied in the target analysis of the data, providing the rate constants reported in Table 1. In the case of $\mathbf{^{Cl}UT}$, fitting the kinetic data requires inclusion of reversible electron injection (k_b, Scheme 1b).

DISCUSSION

Sd is strongly fluorescent in methanol solution; however, its fluorescence is essentially completely quenched when incorporated into DNA as a hairpin linker, irrespective of the identity of the neighboring base pair.[38] Fluorescence quenching is attributed to electron transfer in which **Sd** serves as an electron donor and an adjacent pyrimidine base as an electron acceptor. The free energy for photoinduced electron injection can be estimated using Weller's equation (eq 1)

$$\Delta G_{inj} = -E_S - (E_{rdn} - E_{ox}) + C' \quad (1)$$

DOI: 10.1021/jp512113w
J. Phys. Chem. B 2015, 119, 7673−7680

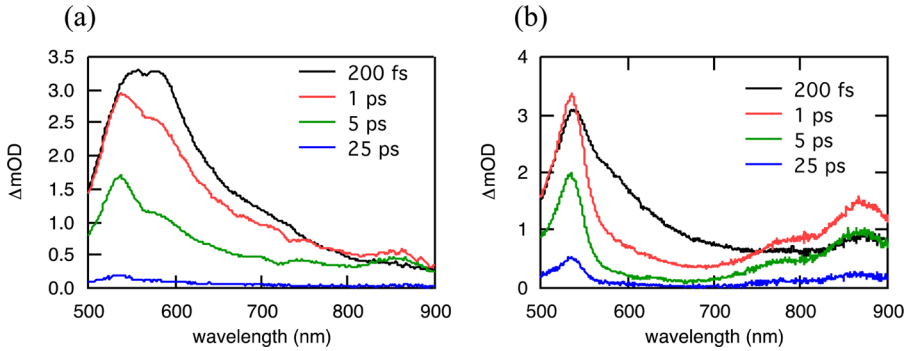

Figure 3. Time-resolved spectra of hairpins (a) **CT** and (b) ^{F}**UT**.

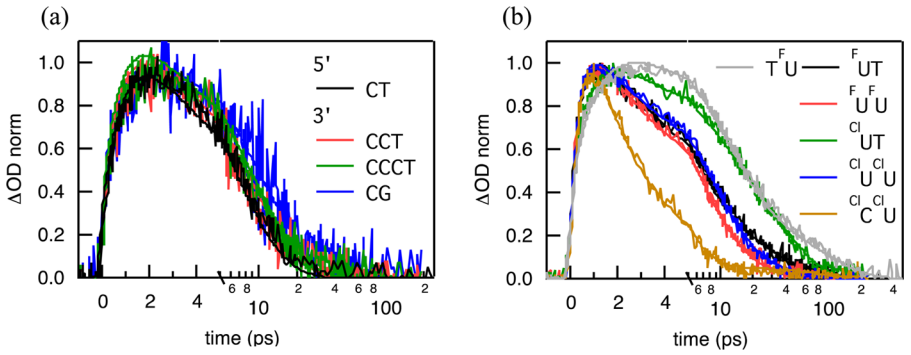

Figure 4. $Sd^{+\bullet}$ formation and decay for (a) hairpins in the C-G series and (b) hairpins in the halo-U series monitored at 860 nm. See Chart 1d,e for hairpin structures.

$$\Delta G_r = E_{rdn} - E_{ox} \quad (2)$$

where E_S and E_{ox} are the singlet energy and oxidation potential of **Sd** (Chart 1a), E_{rdn} is the pyrimidine reduction potential (Chart 1b), and C′ is the Coulomb attraction energy, which can be neglected in highly polar solvents.[47] The free energy of charge recombination (eq 2) can be estimated from the sum of the redox potentials. Calculated values of ΔG_{inj} are exergonic, −0.18 and −0.05 eV for T and C, respectively, and the values of ΔG_r are −3.27 and −3.40 eV for T and C. The values ΔG_{inj} for ^{F}U and ^{Cl}U are more exergonic (−0.46 and −0.57 eV, respectively), based on their reduction potentials that are less negative than those of either T or C (Chart 1b). Because the behavior of these and related electron donor−acceptor systems is determined by the choice of acceptor chromophore and neighboring base pair, the discussion of our results and the related literature is organized by the identity of the neighboring base pair.

Charge Separation and Recombination in the T-A Series. The time-resolved transient absorption spectra for hairpin **T6** are similar to those previously reported for this hairpin[24,25] but have improved signal/noise and include for the first time the 860 nm band as well as the 525 nm band of the Sd cation radical (Figure 1a). This facilitates the analysis of the transient spectra. The resulting value of k_{inj} = 0.64 ps^{-1} is somewhat slower than values based on single-wavelength 575 nm decays (∼2 ps^{-1}). Overlap of the Sd* and $Sd^{+\bullet}$ transient absorption bands at 575 nm provides a plausible reason for the faster k_{inj} values in previous studies. Target analysis provides a value of k_{r1} = 0.034 ps^{-1} for charge recombination of the $Sd^{+\bullet}T^{-\bullet}$ radical ion pair, in good agreement with values based on 525 and 860 nm single-wavelength decays (Figure S5a, Supporting Information) and with previous reports.[24,25]

Values of k_{inj} for **T6**, the **APy**-capped hairpin, and the **2T**-linked hairpin with $(T\text{-}A)_n$ stems, as determined from single-wavelength decays, are 2, 1.8, and 0.84 ps^{-1}, respectively, and their values of k_{r1} are 0.031, 0.14, and 0.029 ps^{-1}.[9,24,26] The values of k_{inj} for the three donors are not well-correlated with estimated values of ΔG_{inj} (−0.18, +0.11, and +0.08 eV for **Sd**, **APy** and **2T**, respectively). The value of k_{r1} is largest for **APy**, in accord with its estimated value of ΔG_r, which is much smaller than those for the other two electron donors (Chart 1b). The limited agreement between the experimental values for electron injection and recombination and the predictions of Marcus theory for electron transfer in prior studies of DNA donor−acceptor systems[26,48] is not surprising in view of the presence of several complicating factors. Among these are the formation of exciplexes with varying degrees of charge-transfer character and hydrophobic interactions between the chromophore and neighboring base pair.

The values of k_{inj} and k_{r1} for hairpins **TA** and **TTA** are the same, within the accuracy of the analysis, as the values for **T6** (Table 1). Thus, the dynamics of charge injection and charge recombination are independent of the number of consecutive T-A base pairs adjacent to the **Sd** linker. Changing the location of T from the 5′-arm to the 3′-arm of the hairpin or replacing the second T-A base pair with a C-G base pair in hairpin **TG** also makes little difference in the values of k_{inj} and k_{r1}. Thus, once injected into T, the electron either remains localized on T or charge delocalization beyond the first base pair has little effect on k_{r1}. In view of the results for the halo-uracils (vide infra), the latter possibility seems unlikely. The slight differences that were observed for **TG** are most likely due to a changed site energy of the first base when the second base is G instead of A. Such effects on site energies have been reported for hole transfer.[49] Thus, the negative charge in the $Sd^{+\bullet}$-$T^{-\bullet}$

DOI: 10.1021/jp512113w
J. Phys. Chem. B 2015, 119, 7673−7680

contact radical ion pair most likely remains localized on the ~30 ps time scale of its decay via charge recombination (Scheme 1a).

Charge Injection and Charge Recombination in the C-G Series. The behavior of the **Sd** hairpins in the C-G series differs considerably from that of the hairpins in the T-A series. Most notably, electron injection in the C-G series is reversible (Scheme 1b), resulting in similar rate constants for electron injection, back electron transfer, and recombination (Table 1). Reversible electron injection has not previously been considered for **Sd**,[24] **APy**,[9] or **2T** hairpins;[26] however, reversible hole injection has been observed for stilbenedicarboxamide (**Sa**) hairpin electron acceptors with adenine electron donors.[25] The calculated values of ΔG_{inj} for charge separation both for **Sd** with C and for **Sa** with A are ~0 eV, appropriate values for reversible exciplex formation.

As is the case for the T-A series hairpins **TA**, **TTA**, and **T6**, the values of k_{inj} and k_{r1} do not change appreciably as the number of consecutive C bases increases for the C series hairpins **CT**, **CCT**, and **CCCT**. The similar values of k_{r1} and the presence of single-exponential charge recombination indicates that the small charge gradient for electron transport from C to T (~0.1 eV, Chart 1b) is not sufficient to promote the occurrence of electron transport from C to T. However, a small degree of charge delocalization by the adjacent T could be responsible for the somewhat larger value of k_{r1} for **CT** than that for **CG**. Alternatively, the larger value of k_{r1} could be a consequence of the effect of the second base on the site energy of the first base, as has been observed for hole transfer.[49]

The values of k_{inj} reported by Fujitsuka and Majima for the **TT** hairpin linker decrease slightly with the number of consecutive C-G base pairs, from 0.35 ps^{-1} for a single C-G to 0.20 ps^{-1} for three C-G's.[26] They report an even smaller decrease in k_{r1} with the number of C-G base pairs. These authors also observe long-lived components of $TT^{+\bullet}$ decay having undetermined lifetimes and amplitudes and suggest that these may arise from electron hopping through poly(C). We observe no long-lived decay component for **Sd**-linked hairpins in either the T-A or C-G series. Dual-exponential charge recombination was observed for an **APy**-capped hairpin having a poly(T-A) stem. The minor longer-lived component (8%, 52 ps) was tentatively attributed to a minor conformation of the capped hairpin.[9]

Charge Injection and Recombination in the Halo-Uracil Series. All of the hairpins possessing either one or two halo-U-A base pairs have faster charge injection rate constants than hairpins in the T-A or C-G series (Table 1). This is consistent with the less negative oxidation potentials of ^{F}U or ^{Cl}U versus T or C. The largest values of k_{inj} are observed for the hairpins that have two consecutive halogenated bases (Table 1). The rate enhancement by ^{F}U observed for ^{F}**UT** is partially attenuated by the intervening T in hairpin **T^{F}U**.

The time-resolved spectra for **T^{F}U** and other members of the halo-uracil series can be fit using Scheme 1c, according to which electron transport from the proximal pyrimidine base to the adjacent pyrimidine base (k_{ET}) competes with the fast charge recombination processes (k_{r1}) and precedes the slower charge recombination processes (k_{r2}). In the case of hairpin ^{Cl}**UT**, the kinetics are further complicated by competition of back electron transfer (k_b, Scheme 1b) with charge recombination and hopping. The values of k_{r1} are similar for all of these hairpins except for **T^{F}U**, which has a smaller recombination rate constant, similar to that of the hairpins in the T series, and for ^{Cl}**C^{Cl}U**, which has a larger rate constant. Values of k_{ET} show the greatest variation, with the largest value being observed for ^{Cl}**UT**, which also undergoes partially reversible electron injection (k_b, Scheme 1b). Quantum yields for electron hopping can be calculated from the rate constants k_{r1} and k_{ET} ($\Phi_{ET} = k_{ET}/(k_{ET} + k_{r1})$). The largest values of Φ_{ET} ($\geq$0.25) are observed for hairpins with a single halo-U in either the first or second base pair. Lower values of Φ_{ET} ($\leq$0.10) are observed for all of the hairpins with halo-U or halo-C in both of the first two base pairs. The transient absorption of $Sd^{+\bullet}$ at 860 nm decays completely within the 2 ns time frame of our measurements (Figure 4). Thus, a second hopping step does not compete effectively with k_{r2} (Scheme 1c).

Multistep electron-transport processes have previously been proposed to account for loss of bromide from ^{Br}U in $T_n{}^{Br}U$ pyrimidine acceptor sequences and in electron-acceptor gradients such as AT**U**^{F}**U**^{Br}**U**.[9,28] However, Ito and co-workers recently reported that gradients based on the reduction potential do not necessarily result in efficient electron transport to ^{Br}U followed by loss of bromide and strand cleavage.[50] We find that the efficiency of electron transport to the second base pair is similar for ^{F}**UT** and ^{Cl}**UT**, which have uphill electron-acceptor gradients, and **T^{F}U**, which has a downhill gradient. This suggests that it is not simply the reduction potential of the pyrimidine that determines the dynamics and efficiency of electron transport in our hairpin systems.

It is, of course, possible that rather than undergoing energetically unfavorable electron transfer from a contact radical ion pair or exciplex (e.g., $Sd^{+\bullet}/{}^{F}U^{-\bullet}$) to a charge-separated ion pair ($Sd^{+\bullet}/{}^{F}U/T^{-\bullet}$), the exciplex relaxes to a triplex in which the negative charge is delocalized over the first two pyrimidines [$Sd^{+\bullet}/({}^{F}U\ T)^{-\bullet}$]. In this case, the electronic coupling between the bases and the stability of the triplex would determine the rate constant for its formation from the exciplex (k_{ET}). A preference for formation of a mixed pyrimidine anion radical ($^{F}U\ T^{-\bullet}$ or $T\ {}^{F}U^{-\bullet}$) versus a homopurine anion radical ($^{F}U\ {}^{F}U^{-\bullet}$ or $TT^{-\bullet}$) could account for the similar values of k_{ET} and Φ_{ET} for **T^{F}U** and ^{F}**UT**, the smaller values for ^{F}**U^{F}U**, and the apparent absence of k_{ET} in the kinetic schemes for our T-A and C-G series. Triplex formation could also account for the similar values of k_{inj}, k_{r1}, and k_{r2} for **APy**-capped hairpins with T^{Br}U and ^{Br}UT pyrimidine sequences.[9]

CONCLUSIONS

In summary, we find that all of the **Sd**-linked hairpins in Chart 1 undergo rapid electron injection (k_{inj}) upon excitation of the **Sd** chromophore. Formation of a contact radical ion pair or exciplex is consistent with the initial changes in the transient absorption spectra observed for all of the hairpins (Figures 1, 3, and S6 (Supporting Information)). Values of k_{inj} are dependent upon the reduction potential of the pyrimidine base in the adjacent base pair, decreasing in the order $^{Cl}U > {}^{F}U > T > C$, and are largest for hairpins having two consecutive halo-pyrimidines adjacent to the **Sd** linker (Table 1). Rate constants for decay of the **Sd** singlet state range from 0.4 to 2.9 ps^{-1}.

The behavior of the radical ion pairs depends upon the identity of the pyrimidine base. The $Sd^{+\bullet}T^{-\bullet}$ radical ion pairs undergo single-exponential charge recombination (Scheme 1a) with decay times of ~30 ps, irrespective of the number of sequential T bases or the identity of the adjacent base (with the exception of ^{F}U). The behavior of the $Sd^{+\bullet}C^{-\bullet}$ radical ion pairs is more complex by virtue of their rapid equilibrium with the **Sd**

DOI: 10.1021/jp512113w
J. Phys. Chem. B 2015, 119, 7673−7680

singlet state (Scheme 1b). The decay times for hairpins having C_nT pyrimidine sequences are ~3 ps, an order of magnitude shorter than those for hairpins having T_n sequences. This difference in the lifetimes of the radical ion pairs for the T-A and C-G series may explain the usual choice of poly(T) sequences for the study of electron transport in DNA[9,28,51] rather than poly(C), as recently suggested.[26]

The behavior of the hairpins possessing halo-pyrimidines in the first and/or second base pair adjacent to the **Sd** linker is the most complex and most promising from the viewpoint of electron transport in DNA over more than a few base pairs. All of these hairpins display nonmonoexponential decay (Scheme 1c) and have slow decay components corresponding to radical ion pair lifetimes ranging from 30 to 90 ps and quantum yields for formation of the long-lived charge-separated state of 0.04−0.26. Hairpin $\mathbf{T^FU}$, which has the combination of slow decay time and large quantum yield best suited to electron transport beyond two base pairs, provides the potential energy gradient utilized by Ito et al. in their strand cleavage studies.[28] Electron injection, transport, and trapping beyond two pyrimidine bases is currently under investigation in our laboratories.

■ ASSOCIATED CONTENT

Supporting Information

Table of mass spectral data and Figures S1−S6 showing HPLC traces, UV and CD spectra, thermal dissociation profiles, kinetic traces for single-wavelength picosecond decay, and femtosecond−picosecond time-resolved broad-band absorption spectra for Sd-linked hairpins. This material is available free of charge via the Internet at http://pubs.acs.org.

■ AUTHOR INFORMATION

Corresponding Authors

*E-mail: fdl@northwestern.edu (F.D.L.).
*E-mail: f.c.grozema@tudelft.nl (F.C.G.).

Author Contributions

[‖]N.G. and T.F. contributed equally.

Notes

The authors declare no competing financial interest.

■ ACKNOWLEDGMENTS

T.F. was supported by a JSPS Research Fellowship. This material is based in part upon work at Northwestern University supported by the U.S. Department of Energy Office of Science, Office of Basic Energy Sciences under Award Number DE-FG02-96ER14604. This work is supported by The Netherlands Organization for Scientific Research (NWO) through a VIDI grant to F.C.G.

■ REFERENCES

(1) Closs, G. L.; Miller, J. R. Intramolecular long-distance electron transfer in organic molecules. *Science* **1988**, *240*, 440−447.
(2) Asaoka, S.; Takeda, N.; Iyoda, T.; Cook, A. R.; Miller, J. R. Electron and hole transport to trap groups at the ends of conjugated polyfluorenes. *J. Am. Chem. Soc.* **2008**, *130*, 11912−11920.
(3) Newton, M. D. Electron transfer: Theoretical models and computational implementation. In *Electron transfer in chemistry*; Wiley-VCH Verlag GmbH: Weinheim, Germany, 2008; pp 2−63.
(4) Siriwong, K.; Voityuk, A. A.; Newton, M. D.; Rösch, N. Estimate of the reorganization energy for charge transfer in DNA. *J. Phys. Chem. B* **2003**, *107*, 2595−2601.
(5) Kawai, K.; Majima, T. Hole transfer kinetics of DNA. *Acc. Chem. Res.* **2013**, *46*, 2616−2625.
(6) Lewis, F. D. Distance-dependent electronic interactions across DNA base pairs. Charge transport, exciton coupling, and energy transfer. *Israel J. Chem.* **2013**, *53*, 350−365.
(7) Ito, T.; Rokita, S. E. Excess electron transfer from an internally conjugated aromatic amine to 5-bromo-2′-deoxyuridine in DNA. *J. Am. Chem. Soc.* **2003**, *125*, 11480−11481.
(8) Manetto, A.; Breeger, S.; Chatgilialoglu, C.; Carell, T. Complex sequence dependence by excess-electron transfer through DNA with different strength electron acceptors. *Angew. Chem., Int. Ed.* **2006**, *45*, 318−321.
(9) Daublain, P.; Thazhathveetil, A. K.; Wang, Q.; Trifonov, A.; Fiebig, T.; Lewis, F. D. Dynamics of photochemical electron injection and efficiency of electron transport in DNA. *J. Am. Chem. Soc.* **2009**, *131*, 16790−16797.
(10) Schwögler, A.; Burgdorf, L. T.; Carell, T. Self-repairing DNA based on a reductive electron transfer through the base stack. *Angew. Chem., Int. Ed.* **2000**, *39*, 3918−3920.
(11) Behrens, C.; Burgdorf, L. T.; Schwogler, A.; Carell, T. Weak distance dependence of excess electron transfer in DNA. *Angew. Chem., Int. Ed.* **2002**, *41*, 1763−1766.
(12) Giese, B.; Carl, B.; Carl, T.; Carell, T.; Behrens, C.; Hennecke, U.; Schiemann, O.; Feresin, E. Excess electron transport through DNA: A single electron repairs more than one UV-induced lesion. *Angew. Chem., Int. Ed.* **2004**, *43*, 1848−1851.
(13) Park, M. J.; Fujitsuka, M.; Kawai, K.; Majima, T. Direct measurement of the dynamics of excess electron transfer through consecutive thymine sequence in DNA. *J. Am. Chem. Soc.* **2011**, *133*, 15320−15323.
(14) Kaden, P.; Mayer-Enthart, E.; Trifonov, A.; Fiebig, T.; Wagenknecht, H.-A. Real-time spectroscopic and chemical probing of reductive electron transfer in DNA. *Angew. Chem., Int. Ed.* **2005**, *44*, 1636−1639.
(15) Harriman, A. Electron tunneling in DNA. *Angew. Chem., Int. Ed.* **1999**, *38*, 945−949.
(16) Kawai, K.; Kimura, T.; Kawabata, K.; Tojo, S.; Majima, T. Excess electron transfer in DNA studied by pulse radiolysis and γ-radiolysis of naphthalimide and iodouridine modified odn. *J. Phys. Chem. B* **2003**, *107*, 12838−12841.
(17) Tainaka, K.; Fujitsuka, M.; Takada, T.; Kawai, K.; Majima, T. Sequence dependence of excess electron transfer in DNA. *J. Phys. Chem. B* **2010**, *114*, 14657−14663.
(18) Vura-Weis, J.; Wasielewski, M. R.; Thazhathveetil, A. K.; Lewis, F. D. Efficient charge transport in DNA diblock oligomers. *J. Am. Chem. Soc.* **2009**, *131*, 9722−9727.
(19) Lewis, F. D.; Zhu, H. H.; Daublain, P.; Fiebig, T.; Raytchev, M.; Wang, Q.; Shafirovich, V. Crossover from superexchange to hopping as the mechanism for photoinduced charge transfer in DNA hairpin conjugates. *J. Am. Chem. Soc.* **2006**, *128*, 791−800.
(20) Blaustein, G. S.; Lewis, F. D.; Burin, A. L. Kinetics of charge separation in poly(A)−poly(T) DNA hairpins. *J. Phys. Chem. B* **2010**, *114*, 6732−6739.
(21) Grozema, F. C.; Tonzani, S.; Berlin, Y. A.; Schatz, G. C.; Siebbeles, L. D. A.; Ratner, M. A. Effect of structural dynamics on charge transfer in DNA hairpins. *J. Am. Chem. Soc.* **2008**, *130*, 5157−5166.
(22) Renaud, N.; Berlin, Y. A.; Lewis, F. D.; Ratner, M. A. Between superexchange and hopping: An intermediate charge-transfer mechanism in poly(A)−poly(T) DNA hairpins. *J. Am. Chem. Soc.* **2013**, *135*, 3953−3963.
(23) Zhang, Y.; Liu, C.; Balaeff, A.; Skourtis, S. S.; Beratan, D. N. Biological charge transfer via flickering resonance. *Proc. Natl. Acad. Sci. U.S.A.* **2014**, *111*, 10049−10054.
(24) Lewis, F. D.; Liu, X.; Miller, S. E.; Hayes, R. T.; Wasielewski, M. R. Dynamics of electron injection in DNA hairpins. *J. Am. Chem. Soc.* **2002**, *124*, 11280−11281.
(25) Lewis, F. D.; Zhu, H.; Daublain, P.; Fiebig, T.; Raytchev, M.; Wang, Q.; Shafirovich, V. Crossover from superexchange to hopping as the mechanism for photoinduced charge transfer in DNA hairpin conjugates. *J. Am. Chem. Soc.* **2006**, *128*, 791−800.

DOI: 10.1021/jp512113w
J. Phys. Chem. B 2015, 119, 7673−7680

(26) Park, M. J.; Fujitsuka, M.; Kawai, K.; Majima, T. Excess-electron injection and transfer in terthiophene-modified DNA: Terthiophene as a photosensitizing electron donor for thymine, cytosine, and adenine. *Chem.—Eur. J.* **2012**, *18*, 2056−2062.
(27) Park, M. J.; Fujitsuka, M.; Kawai, K.; Majima, T. Corrigendum: Excess-electron injection and transfer in terthiophene-modified DNA: Terthiophene as a photosensitizing electron donor for thymine, cytosine, and adenine. *Chem.—Eur. J.* **2012**, *18*, 7326−7326.
(28) Ito, T.; Hamaguchi, Y.; Tanabe, K.; Yamada, H.; Nishimoto, S.-i. Transporting excess electrons along potential energy gradients provided by 2′-deoxyuridine derivatives in DNA. *Angew. Chem., Int. Ed.* **2012**, *51*, 7558−7561.
(29) Vura-Weis, J.; Wasielewski, M. R.; Thazhathveetil, A. K.; Lewis, F. D. Efficient charge transport in DNA diblock oligomers. *J. Am. Chem. Soc.* **2009**, *131*, 9722−9727.
(30) Thazhathveetil, A. K.; Trifonov, A.; Wasielewski, M. R.; Lewis, F. D. Increasing the speed limit for hole transport in DNA. *J. Am. Chem. Soc.* **2011**, *133*, 11485−11487.
(31) Sieber, R. H. Reaktionen von chloracetaldehyd mit aromatischen kohlenwasserstoffen, phenolen und phenoläthern. *Liebigs Ann. Chem.* **1969**, *730*, 31−46.
(32) Letsinger, R. L.; Wu, T. Use of a stilbenedicarboxamide bridge in stabilizing, monitoring, and photochemically altering folded conformations of oligonucleotides. *J. Am. Chem. Soc.* **1995**, *117*, 7323−7328.
(33) Kanamori, T.; Masaki, Y.; Mizuta, M.; Tsunoda, H.; Ohkubo, A.; Sekine, M.; Seio, K. DNA duplexes and triplex-forming oligodeoxynucleotides incorporating modified nucleosides forming stable and selective triplexes. *Org. Biomol. Chem.* **2012**, *10*, 1007−1013.
(34) Kang, J. I.; Burdzy, A.; Liu, P.; Sowers, L. C. Synthesis and characterization of oligonucleotides containing 5-chlorocytosine. *Chem. Res. Toxicol.* **2004**, *17*, 1236−1244.
(35) Snellenburg, J. J.; Laptenok, S. P.; Seger, R.; Mullen, K. M.; van Stokkum, I. H. M. Glotaran: A java-based graphical user interface for the R package TIMP. *J. Stat. Software* **2012**, *49*, 1−22.
(36) Mullen, K. M.; van Stokkum, I. H. M. TIMP: An R package for modeling multi-way spectroscopic measurements. *J. Stat. Software* **2007**, *18*, 1−46.
(37) van Stokkum, I. H. M.; Larsen, D. S.; van Grondelle, R. Global and target analysis of time-resolved spectra. *Biochim. Biophys. Acta, Bioenerg.* **2004**, *1657*, 82−104.
(38) Lewis, F. D.; Wu, Y.; Liu, X. Synthesis, structure, and photochemistry of exceptionally stable synthetic DNA hairpins with stilbene diether linkers. *J. Am. Chem. Soc.* **2002**, *124*, 12165−12173.
(39) Stolarski, R.; Egan, W.; James, T. L. Solution structure of the ecori DNA octamer containing 5-fluorouracil via restrained molecular dynamics using distance and torsion angle constraints extracted from NMR spectral simulations. *Biochemistry* **1992**, *31*, 7027−7042.
(40) Sahasrabudhe, P. V.; Pon, R. T.; Gmeiner, W. H. Effects of site-specific substitution of 5-fluorouridine on the stabilities of duplex DNA and RNA. *Nucleic Acids Res.* **1995**, *23*, 3916−3921.
(41) Theruvathu, J. A.; Kim, C. H.; Rogstad, D. K.; Neidigh, J. W.; Sowers, L. C. Base pairing configuration and stability of an oligonucleotide duplex containing a 5-chlorouracil-adenine base pair. *Biochemistry* **2009**, *48*, 7539−7546.
(42) Theruvathu, J. A.; Yin, Y. W.; Pettitt, B. M.; Sowers, L. C. Comparison of the structural and dynamic effects of 5-methylcytosine and 5-chlorocytosine in a CPG dinucleotide sequence. *Biochemistry* **2013**, *52*, 8590−8598.
(43) Hara, M.; Tojo, S.; Majima, T. Formation efficiency of radical cations of stilbene and methoxy-substituted stilbenes during resonant two-photon ionization with a XECL excimer laser. *J. Photochem. Photobiol., A* **2004**, *162*, 121−128.
(44) Steckhan, E.; Yates, D. A. Spectroelectrochemical studies of olefins-ii a technique for acquisition of the ultraviolet−visible spectra of electrogenerated reactive intermediates. *Ber. Bunsen-Ges. Phys. Chem.* **1977**, *81*, 369−374.
(45) Shida, T. *Electronic Absorption Spectra of Radical Ions*; Elsevier: Amsterdam, The Netherlands, 1988.
(46) Grozema, F. C.; Candeias, L. P.; Swart, M.; van Duijnen, P. T.; Wildeman, J.; Hadziioanou, G.; Siebbeles, L. D. A.; Warman, J. M. Theoretical and experimental studies of the opto-electronic properties of positively charged oligo(phenylene vinylene)s: Effects of chain length and alkoxy substitution. *J. Chem. Phys.* **2002**, *117*, 11366−11378.
(47) Weller, A. Photoinduced electron transfer in solution: Exciplex and radical ion pair formation free enthalpies and their solvent dependence. *Z. Phys. Chem., Neue Folge* **1982**, *133*, 93−98.
(48) Lewis, F. D.; Kalgutkar, R. S.; Wu, Y.; Liu, X.; Liu, J.; Hayes, R. T.; Wasielewski, M. R. Driving force dependence of electron transfer dynamics in DNA. *J. Am. Chem. Soc.* **2000**, *122*, 12346−12351.
(49) Senthilkumar, K.; Grozema, F. C.; Guerra, C. F.; Bickelhaupt, F. M.; Lewis, F. D.; Berlin, Y. A.; Ratner, M. A.; Siebbeles, L. D. Absolute rates of hole transfer in DNA. *J. Am. Chem. Soc.* **2005**, *127*, 14894−903.
(50) Ito, T.; Kurihara, R.; Utsumi, N.; Hamaguchi, Y.; Tanabe, K.; Nishimoto, S.-i. Electron transport through 5-substituted pyrimidines in DNA: Electron affinities of uracil and cytosine derivatives differently affect the apparent efficiencies. *Chem. Commun.* **2013**, *49*, 10281−10283.
(51) Elias, B.; Shao, F. W.; Barton, J. K. Charge migration along the DNA duplex: Hole versus electron transport. *J. Am. Chem. Soc.* **2008**, *130*, 1152−1153.

DOI: 10.1021/jp512113w
J. Phys. Chem. B 2015, 119, 7673−7680